Preparation and characterisation of epoxy/alumina polymer nanocomposites

B.B. Johnsen*, T.R. Frømyr, T. Thorvaldsen, T. Olsen

Norwegian Defence Research Establishment (FFI), Kjeller, Norway

*Corresponding author. Email: bernt.johnsen@ffi.no

Postal address: Norwegian Defence Research Establishment (FFI), P.O. Box 25, NO-2027 Kjeller, Norway

Dette er en postprint-versjon/This is a postprint version.
DOI til publisert versjon/DOI to published version: 10.1080/15685543.2013.815603

Preparation and characterisation of epoxy/alumina polymer nanocomposites

The effect of adding nanosized alumina fillers of both fibre-like and spherical shapes to an epoxy polymer has been investigated. The alumina was dispersed in the epoxy hardener using two different sonication techniques. A high degree of dispersion was difficult to obtain and agglomerates were observed in the nanocomposites. Nevertheless, particle size analysis showed an effect of the sonication technique, resulting in a higher degree of dispersion. Mechanical testing and dynamic mechanical analysis revealed that the stiffness of the epoxy polymer could be significantly improved using only small amounts of alumina, even when a significant part of the filler was in an agglomerated state. Also, the experimental results from tensile testing agreed well with mathematical models at low filler concentrations.

Keywords: epoxy; alumina; nanocomposites; dispersion; reinforcement; mathematical modelling

1 Introduction

Extensive research is being conducted on polymer composites reinforced with rigid nanoparticles. Engineering polymers, such as epoxy, have many excellent material properties but they are, however, generally brittle materials. Therefore, to fully exploit the properties, epoxy polymers often need to be reinforced by adding either micro- or nanosized particles. Inorganic particles have a much higher stiffness than the polymer matrix and may improve the stiffness, and other properties of the materials [1]. A range of inorganic nanoparticles may be used as reinforcements, including carbon nanotubes [2-4], nanofibres [4], clay [4;5], and silica [6;7]. According to Fu *et al.* [1], the inorganic fillers can modify the stiffness, strength and toughness of polymers. In general, the mechanical properties of particulate-polymer composites depend primarily on the particle size, the particle/matrix interface adhesion and the particle loading. The stiffness depends significantly on the particle loading – not the particle/matrix adhesion.

DOI til publisert versjon/DOI to published version: 10.1080/15685543.2013.815603

The strength and toughness are strongly affected by all three factors – particularly the particle/matrix adhesion and thus the stress transfer between the particles and the matrix.

The main difference between using nanosized fillers, compared to microsized fillers, is the much higher specific surface area of the nanomaterials. The higher surface area also means that there is a lot more polymer interphase in the nanocomposite, and that the composite properties may become more dominated by this interphase. Below a critical particle size, the composite stiffness may be greatly enhanced due to the effect of the particle size, probably caused by the much larger surface areas imparting what is called a "nano-effect" [1;4;5]. Here, the polymer interphase surrounding the particles gradually dominate the material properties leading to, for example, changes in the glass transition temperature of the polymer [5;8].

A good dispersion of the nanoparticles in the polymer is usually regarded as a prerequisite to fully exploit their potential benefits. The presence of agglomerates will limit the effect of adding the nanofiller. Also, Nairn [9] suggests, based on results from modelling, that the interface may be more important for nanosized fillers than for larger fillers, and that effective reinforcement is dependent on interfacial compatibility. Nairn also suggests that only modest reinforcement effects can be expected at low volume fractions. At very low volume fractions, the need for high fibre aspect ratios suggest that stiff nanocomposites can not be produced. There is a better potential at higher volume fractions where the aspect ratio requirements are much lower. Still, a lot of published work on nanocomposites is focusing on the low volume fraction range. For example, for carbon nanotubes, typical volume fractions that are studied are in the range from 0.1 to 1.0 vol%.

The use of nanosized alumina to improve the mechanical properties of epoxy polymers has to some extent been studied [10-15]. Alumina has a tensile modulus of around 386 GPa, which is at least two orders of magnitudes higher than most polymers, and should therefore have the potential to significantly stiffen epoxy polymers, which typically have a tensile modulus of around 2.5-3.5 GPa. Brown and Ellyin [10;11] investigated the mechanical behaviour of epoxy reinforced with alumina nanofillers of different shapes. The alumina was dispersed into the polymer by mixing it into the hardener using sonication. Both the tensile stiffness and strength of the epoxy was improved by adding small volume fractions of nanofiller. The reinforcing effect was highest for nanofibres, compared to spherical nanoparticles, and the tensile stiffness increased by up to 19% by adding less than 1.5 vol% of the nanofibre. Similar studies were conducted by Miyagawa *et al.* [12] and Yang *et al.* [14], yielding similar conclusions. The tensile strength and elastic modulus was increased by up to 37% and 60%, respectively, by adding 1 wt% of fibre-like alumina. Positive effects on the composite tensile strength after silane surface treatment of the alumina has also been observed [10;11].

In this study, we have investigated the dispersion and reinforcing effect of fibre-like whiskers and spherical nanosized alumina on an epoxy polymer. The alumina nanofillers are originally in a highly agglomerated state, and two different sonication techniques were used for dispersion. Both fibre-like and spherical alumina was investigated to see if there was any effect of the shape of the filler on the properties of the nanocomposites. The mechanical and thermal properties were determined using tensile and dynamic mechanical testing. Electron microscopy was conducted to investigate the microstructure of the materials, and to be able to correlate the microstructure to the mechanical properties. The alumina was also surface-modified

using a silane to investigate whether this could improve the strength of the alumina/polymer interface and thereby improve the properties of the composites. For further analysis of the stiffness of the nanocomposites, the Young's modulus in the direction of the applied load was compared to mathematical models.

2 Experimental

2.1 Materials

The epoxy polymer investigated in this work was Araldite LY 556/Aradur 917/Accelerator DY 070 from Huntsman. LY 556 is a bisphenol A based epoxy resin, Aradur 917 is an acid anhydride hardener and DY 070 is an imidazole accelerator. Epoxy polymers typically have a Poisson's ratio, ν, of 0.35 [6].

Two different types of nanosized alumina (aluminium oxide, Al_2O_3) (Sigma Aldrich) fillers were employed: (1) Fibre-like whiskers and (2) spherical particles, both supplied as dry powders. The whiskers had a diameter of 2-4 nm and a length of 200-400 nm. The supplier estimated the aspect ratio to be >100. The spherical γ-alumina particles had a diameter of <50 nm and a surface area of >40 m^2/g. The densities of α-alumina and γ-alumina are 3.95 g/cm^3 and 3.47 g/cm^3, respectively [16]. Here, we assume that both alumina fillers are γ-alumina. Alumina typically has a Young's modulus of 386 GPa, and a Poisson's ratio of 0.22 [17]. γ-Glycidyloxypropyltrimethoxysilane (GPS) (Sigma Aldrich) was used for surface treatment of the alumina.

2.2 Nanocomposite preparation

Neat epoxy polymer specimens were prepared by first mixing the epoxy resin, the anhydride hardener and the imidazole accelerator at the ratio 100:90:1 by weight. The

blend was stirred manually, and then cast in cylindrical metal moulds that had been coated with a release agent. The blend was cured for 4 hours at 80^{o}C and 8 hours at 140^{o}C.

The alumina was dispersed in the anhydride hardener of the epoxy polymer by sonication [18]. Sonication was performed in either a bath ultrasonicator (Bandelin Sonorex Digital 10P, 35 kHz, 480 W) or a horn-type ultrasonicator (Branson Digital Sonifier® S-450D, 25 kHz, 400 W). The bath sonicator was run at maximum power, and the whole dispersion was immersed into the bath. During horn sonication, the tip of the horn was placed into the dispersion, and the power delivered was controlled by setting the amplitude at the tip of the resonating horn to 20%. The specific energy input was much higher for the horn sonicator. For the bath sonicator the energy input after 1 hour was estimated to be 0.5 kJ/g, while the corresponding energy input on the horn sonicator was 19 kJ/g. The temperature of the dispersion was kept constant at approximately 50^{o}C in both cases. After sonication for 1 hour, epoxy and accelerator were added to the alumina/anhydride dispersion. The mixture was rigorously stirred, then cast in the metal moulds and finally cured. Some sediments of agglomerated alumina were in many cases observed in the cured cylindrical rods. Thus, there was clearly a sedimentation process of alumina agglomerates that took place prior to the gelation of the epoxy polymer. Since the sediment was at the end of the rods, it was removed and not included in any of the tested specimens. Nanocomposites with nominal filler contents up to 5.00 wt% were prepared. Specimens with higher filler contents were difficult to prepare due to the increasing viscosity of the alumina/anhydride dispersion and the increasing tendency to sedimentation of the filler.

The spherical alumina particles were surface-modified using GPS, following a procedure found in the literature [19-21]. The surface treatment was done by first

adding 10 g of alumina filler to 100 ml toluene. The mixture was sonicated for 5 hours on the bath sonicator, after which the GPS was added at a ratio of 1:1.5 with respect to the amount of alumina. The solution was refluxed for 15 hours, and the alumina filler was repeatedly centrifuged and washed with fresh toluene, before drying in an oven at 110˚C for 3 hours. Successful surface modification was confirmed by Fourier transform infrared spectroscopy and thermogravimetric analyses of non-modified and surface-modified alumina particles. Nanocomposites reinforced with the surface-modified alumina fillers were prepared following the same procedure as for the non-modified alumina fillers. A list of all the different types of nanocomposites that were prepared is given in (Table 1).

2.3 Characterisation

Scanning electron microscopy (SEM) was performed on a Hitachi SU6600 Schottky Field Emission Analytical SEM. The specimens were not coated prior to imaging. The secondary electrons detector was employed to obtain the images.

Tensile testing was conducted on rod-type specimens, as illustrated in (Figure 1), employing a MTS Material Testing Systems 810 testing machine. The specimens were prepared by machining of the cylindrical rods of the nanocomposites, creating a middle part with a reduced cross-sectional area, and tested at a crosshead speed of 5 mm/min. During the testing, the specimens were attached to a pair of self-aligning grips. This allowed the specimens to move freely into alignment so that the load was applied in the direction of the long axis. A clip-gauge extensometer was used for recording the strain. The middle part of the specimen was 4 mm in diameter, and the gauge length was 25 mm. Values for the tensile modulus of elasticity, E, the maximum tensile stress, or the tensile strength, σ_{max}, and the maximum elongation, or tensile strain at break, ε_{max}, were determined. E was determined from the linear part of the stress-

strain curve in the strain range from 0.1% to 0.3%. Average values of five replicate specimens are reported.

Dynamic mechanical analysis (DMA) was performed on a DMA 2980 Dynamic Mechanical Analyzer from TA Instruments. Rectangular specimens with the dimensions 3 mm × 3 mm × 30 mm were employed. The analysis was conducted with a single cantilever clamp, which had a specimen free length of 10 mm. The oscillation frequency was 1 Hz, and the heating rate was 5^{o}C/min. The value of the storage modulus, E', was measured at a temperature of 30^{o}C, and the value of the glass transition temperature, T_g, of the epoxy polymer is reported as the peak value of the loss modulus, E''.

The density of the nanocomposites were measured according to ASTM D 792-08 [22]. The density was in the range from 1.20 g/cm^3 for the neat epoxy polymer to 1.23 g/cm^3 for the nanocomposite with the highest measured value.

The alumina/anhydride dispersions were investigated with transmission light microscopy on thin films of the dispersions that were deposited between two glass plates. Dispersions similar to those used to prepare the nanocomposites were employed.

The particle size distribution of dispersions of spherical alumina particles were characterised in a disc centrifuge (DCF) (DC24000, CPS Instruments, Inc.). The disc centrifuge separates particles by size using differential centrifugal sedimentation (DCS) in a liquid with a density gradient. A 5-15 vol% gradient of Halocarbon 1.8 (Solvadis) in methyl isobutyl ketone (MIBK) (>99% Merck) was formed with a linear density gradient former (Beckmann), and gave several hours of stable operation at the maximum speed of 24000 rpm. The size in the particle size distributions is reported as a Stokes spherical diameter, D_{ST}, which is the equivalent hard sphere diameter having the same sedimentation time as the measured particles.

Anhydride dispersions were diluted 1:10 in MIBK solution with a 0.1 wt% polymer stabilizer (Disperbyk 2070, BYK-Chemie GmbH) and sonicated one min prior to analysis. Furthermore, a low concentration model system containing 0.1 wt% spherical alumina in MIBK and 0.2 wt% Disperbyk 2070 was prepared to compare the effect of bath and horn sonication, eliminating the dilution step necessary for the anhydride dispersions.

3 Dispersion of alumina nanofillers

3.1 Microscopy

Scanning electron micrographs of the two as-received alumina nanofillers employed in this study are shown in (Figure 2(a)-(d)), revealing that the fillers reside in a highly agglomerated state. The resolution of the micrographs is too low to detect individual whiskers or particles, but the agglomeration indicates that relatively strong intermolecular forces are acting between the whiskers, and also between the 50 nm particles. This is expected to represent a challenge with respect to the dispersion of alumina in a given solvent, e.g. epoxy curing agents, as large forces are required to separate the particles from one another. In fact, difficulties to obtain a high degree of dispersion were observed in this study, as will be explained in more detail below.

Some sedimentation of alumina was observed during the preparation of the nanocomposites. This sedimentation is illustrated in (Figure 3), where the state of alumina/anhydride dispersions 30 min after mixing and 30 min after bath sonication for 1 hour is shown. After mixing, there is sedimentation of alumina, which is as expected due to the agglomerated state. After bath sonication, the dispersions are more stable and have a milky-white appearance, which is indicating that the large agglomerates have

been broken into smaller particles. Nevertheless, some sedimentation still took place, and this was also observed during the preparation of the nanocomposite specimens.

Alumina/anhydride dispersions similar to those used to prepare the nanocomposites were investigated by microscopy by taking out a small sample before and after sonication. From (Figure 4), which is illustrating dispersions with relatively high alumina concentrations, it is obvious that the sonication process, at least to some extent, aids in breaking up the large alumina agglomerates. Moreover, most of the large agglomerates seem to have been broken up. In general, fewer large agglomerates are observed after horn sonication, compared to bath sonication, indicating that the higher energy input used in the horn sonication is more efficient for dispersion of the alumina fillers. The thin films of the dispersions in (Figure 4) were placed between two glass plates. This may result in some flow of the dispersion, with the subsequent result of local concentration gradients of alumina.

In (Figure 2(e)), the surface-modified 50 nm alumina particles are shown. These particles were sonicated during the surface treatment procedure, and the large micron-sized particles in (Figure 2(c)) were broken up into much smaller fragments. This can also be seen from (Figure 4(g)). However, it seems that the removal of the solvent in which the surface treatment was conducted, may have led to some re-agglomeration of the alumina, as relatively large clumps, or agglomerates, were observed. Nevertheless, after dispersion in the anhydride, these agglomerates were no longer observed in the alumina/anhydride dispersions, indicating weaker interfacial interactions between the particles after surface-modification.

3.2 Particle size distributions of spherical alumina filler

Particle size distributions of dispersions of the as-received spherical alumina particles were determined by differential centrifugal sedimentation. In contrary to most other

equivalent techniques, DCS is especially suitable for detecting smaller primary particles in an agglomerated suspension [18]. Therefore, particle size distributions in the range from 20 nm to 1 μm were measured to observe the amount of fully dispersed 50 nm alumina particles in sonicated suspensions.

The model system of 0.1 wt% spherical alumina in MIBK is shown in curves 1-3 in (Figure 5). The particle size distributions after bath sonication are bi-modal with a maximum at 400-500 nm and a shoulder at approximately 100 nm. The total mass in the size range increases with sonication time, which is a clear indication that agglomerates larger than 1 μm are still present in the suspensions. The larger agglomerates are not detectable during the analysis, but as they break up into agglomerates smaller than 1 μm, they are made detectable. However, the particle size distributions do not reveal any 50 nm primary particles, even after 1 hour of sonication on the bath.

A further 10 min sonication with a horn at 20% amplitude revealed that the colour of the suspension changed slightly towards grey. This is in line with observations of the anhydride dispersions, and has been explained as lattice strain in the alumina [23]. The particle size distribution changed significantly after the horn sonication, as seen in curve 3 in (Figure 5). The total mass was increased, and a peak at 50 nm was now present. This peak is presumably primary 50 nm alumina particles. However, a horn sonicator will always, to some extent, contaminate the suspension with metal particles because of erosion of the tip [24]. In our case, these particles are also around 50 nm but the concentration was approximately two orders of magnitude lower than for the primary alumina particles. The contamination should therefore not have any practical influence on the measurements.

Investigations of entangled multiwall carbon nanotubes have shown that the concentration of fully dispersed particles are primarily controlled by the sonication

energy input [18]. The specific energy input of the bath after 1 hour was estimated to 0.5 kJ/g, in contrast to 3.2 kJ/g after only 10 minutes of horn sonication. The increased energy input was necessary to produce the fraction of fully dispersed 50 nm alumina particles. In comparison, more than 6 hours of sonication in the bath is needed to create the same specific energy input.

Horn sonication is not independent of the sample volume, as the ultrasonic wave originates at the resonating horn tip and the intensity decreases with distance from this tip. The sample volume of the alumina/anhydride dispersions, later used for the preparation of epoxy nanocomposites, was much larger than the MIBK volume and, consequently, the specific energy input per time was lower. Curve 4 in (Figure 5) shows a 2.0 wt% alumina/anhydride dispersion after 1 hour of horn sonication. Most noteworthy is the lack of signal at 50 nm, while the concentration at 100-200 nm is higher than in the MIBK system. Since a polymer stabilizer was only added to the MIBK system, it is reasonable to suspect that re-agglomeration of primary alumina particles to some extent takes place in the alumina/anhydride dispersions. The re-agglomerated particles will then be detected at sizes higher than 50 nm.

By integrating curve 3 and 4 from 20 nm to 500 nm, the total mass was 16 µg and 12 µg for the MIBK and the anhydride system, respectively. The specific energy input was the same in both systems, but the initially injected concentration of the anhydride system was, however, twice the concentration of the MIBK system. This indicates that the sonication was more efficient in the MIBK system.

No meaningful results could be obtained for the dispersions containing alumina whiskers. This is in part due to the very small diameter of 2-4 nm of the whiskers, which results in a correspondingly small hydrodynamic diameter, being too small for detection of individual whiskers.

4 Characterisation of nanocomposites

4.1 Tensile testing

Tensile testing of the neat epoxy and the nanocomposites were conducted to determine the mechanical effect of adding the two different alumina nanofillers. The test results from the composites that were dispersed using the bath sonicator are given in (Table 2), while the test results after dispersion using the horn sonicator are given in (Table 3). The test results are also illustrated in (Figure 6). The location of the fracture was always in the middle part of the specimen with the reduced cross-sectional area. Typically, but not always, the fracture was relatively close to the edge of this middle part.

For all nanocomposites, the tensile modulus, E, was increased, or at least equal, to the neat epoxy. The highest increase was seen for the specimen containing 5.0 wt% whiskers dispersed using the bath sonicator ("NT-whiskers-bath"), where the tensile modulus was increased from 3120 MPa for the neat epoxy polymer, to 3540 MPa for the composite. This is an increase of around 13%, and comparable to what was observed by Brown and Ellyin [10;11]. It is noteworthy that the addition of only 0.1 wt% whiskers increased the tensile modulus to 3310 MPa. The dispersion of the 50 nm particles using the bath sonicator did not have the same effect on the tensile modulus. Here, the modulus was only slightly increased with increasing concentration of alumina.

The different effect of dispersing the alumina using bath or horn sonication can clearly be seen when considering the 50 nm particles at concentrations of around 1 wt%. The mechanical properties of the nanocomposite were much better after dispersion using the horn sonicator, compared to using the bath sonicator, see (Table 2) and (Table 3). The most obvious explanation for this behaviour is that the large agglomerates of the as-received filler, as observed in (Figure 2) and (Figure 4), are not broken up to the same extent when using the bath sonicator. More and larger agglomerates seemed to be

present after using the bath sonicator, as was illustrated in the microscopy of the alumina/anhydride dispersions in (Figure 3). Scanning electron micrographs of the fracture surfaces of the composites also gave supporting evidence of this assumption. In the fracture surface of the neat epoxy no inclusions or agglomerates were observed, see (Figure 7). However, in the fracture surface of the nanocomposite ("NT-50nm-bath"), see (Figure 8(a)), features of what appears to be remains of large alumina agglomerates were observed after bath sonication. These features were not observed after dispersion using the horn sonicator ("NT-50nm-horn"), see (Figure 8(b)). The latter fracture surface was also rougher. The agglomerates of the 50 nm alumina filler are relatively weak. As an example, they easily fracture when a low compressive force is applied to them. Thus, the presence of these weak agglomerates in the epoxy polymer would act as sites where crack propagation could take place relatively easily, without absorbing a lot of energy, resulting in lower mechanical properties. The same strong effect of the type of sonication was not seen for the whiskers, where the alumina particles are likely to reside in a more strongly agglomerated state, meaning that they are acting more like micron-sized particles in the epoxy polymer.

Another interesting observation when using the horn sonicator, was the apparent maximum in tensile modulus for both the whiskers ("NT-whiskers-horn") and the 50 nm particles ("NT-50nm-horn"). Only two concentrations of each non-treated filler was prepared, but the composites containing around 1 wt% alumina gave a higher modulus than the composites containing around 3 wt%. Normally, one would expect a higher modulus at higher concentrations. This behaviour could be related to the energy intensity decrease with distance around the horn tip, as explained in Section 3.2. This effect may be enhanced at higher concentrations of alumina, since the ultrasonic wave responsible for the dispersion process may be dampened significantly more than at

lower concentrations. When using the bath sonicator, on the other hand, the energy density is distributed more uniformly throughout the whole dispersion as it is immersed into a water bath.

Surface treatment of the 50 nm particles with GPS silane seemed to have a positive effect on the strength, σ_{max}, and the elongation, ε_{max}, of the nanocomposites. In general, the tensile strength was reduced for all the nanocomposites by up to 15% compared to the neat epoxy. This could be explained by the presence of agglomerates that are creating defects which act as initiation sites for crack propagation. The only exception from this was the specimen with 1.0 wt% of the surface-modified particulate filler dispersed using the horn sonicator ("GPS-50nm-horn"), which had a higher strength than the neat epoxy polymer. Furthermore, the elongation at break was always reduced upon addition of the nanofillers. However, for the surface-modified particles, the reduction was lower than for the non-modified particles at similar concentrations of alumina. For example, the effect was most pronounced for the specimen with 3.0 wt% surface-modified alumina dispersed using the bath sonicator ("GPS-50nm-bath").

4.2 DMA

The same nanocomposites as those investigated by tensile testing, were also investigated by DMA. DMA-curves for selected specimens are shown in (Figure 9). Much lower values of the storage modulus, E', compared to the tensile modulus, E, were measured. When conducting the DMA testing in the single cantilever mode, there is a combined explanation for this. First, the measured stiffness is multiplied by a geometry calibration factor in the DMA software. This introduces an uncertainty. Second, the small span length leads to a significant contribution from shear forces during the testing. This lowers the measured value of E' since the shear modulus, G, is

lower than the tensile modulus, E. However, a comparison of the values of E' between the different specimens is still valid.

The DMA measurements confirmed the results of the tensile testing. The storage modulus, E', of the neat epoxy polymer was 2050 MPa, and this value was increased upon addition of alumina. For the composites containing whiskers that had been dispersed using the bath sonicator ("NT-whiskers-bath"), values of E' of 2310 MPa and 2510 MPa were obtained for concentrations of 1.0 wt% and 5.0 wt%, respectively. The value of E' was also increased for the spherical 50 nm alumina, and even more so than what was observed by tensile testing. For the composite containing 4.0 wt% non-treated alumina ("NT-50nm-bath"), 2380 MPa was obtained, while for 3.0 wt% surface-modified alumina ("GPS-50nm-bath"), 2320 MPa was obtained.

Dispersion using the horn sonicator gave slightly lower values for E', compared to sonication using the bath, but the same trends as those measured by tensile testing were confirmed. Nevertheless, the stiffness of the composite containing 1.0 wt% of the spherical 50 nm alumina ("NT-50nm-horn") was not as high at 2120 MPa. The highest value of E' was measured for the composite containing 2.9 wt% whiskers ("NT-whiskers-horn") at 2230 MPa.

The glass transition temperature, T_g, did not vary significantly between the neat epoxy polymer and the nanocomposites prepared by bath sonication. The value of the T_g was within 156 ± 2^{o}C, with the exception of the composite containing 5.0 wt% whiskers ("NT-whiskers-bath"), giving a value of 152^{o}C. After horn sonication, the T_g was generally slightly higher at 161 ± 1^{o}C (including a neat epoxy polymer sample that was subjected to the sonication procedure, but without the presence of any filler). The exceptions were the composites containing 2.9 wt% particulate and 2.9 wt% fibre-like fillers, respectively, where the value was 157^{o}C. Hence, there was no indication of a

Dette er en postprint-versjon/This is a postprint version.
DOI til publisert versjon/DOI to published version: 10.1080/15685543.2013.815603

"nano-effect" giving a higher T_g for the composites. Neither is the cured epoxy polymer negatively affected, although there might be a small decrease in T_g at the higher filler concentrations investigated here.

4.3 SEM

Scanning electron micrographs of fracture surfaces of the tensile test specimens of the neat epoxy polymer are shown in (Figure 7). The fracture surface of the neat epoxy polymer was relatively smooth around the crack initiation site, and more rough and three-dimensional towards the opposite side of the specimen. This corresponds well to previously reported fracture surfaces of unfilled epoxies with blunt pre-cracks [25]. Indeed, this was quite typical also for the nanocomposites containing the alumina fillers. However, the fracture surfaces of the nanocomposites usually had a much more rough appearance, although to a varying extent, see (Figure 8). This is what is expected for a polymer containing rigid inclusions. The inclusions, in this case most probably agglomerated alumina particles of different sizes, forces the growing crack to deflect in its path, thus creating the rough fracture surfaces. In fact, in many of the nanocomposites, significant amounts of alumina agglomerates could be observed. For example, in the fracture surface of the nanocomposite containing whiskers dispersed on the bath ("NT-whiskers-bath"), both agglomerates and what appeared to be relatively epoxy-rich regions were observed, see (Figure 8(c)). Also, debonding between the agglomerated whiskers and the epoxy was observed. The whiskers that were dispersed using the horn ("NT-whiskers-horn") gave a more smooth fracture surface with fewer agglomerates, indicating that the horn sonicator is more efficient for dispersing the whiskers. In general, a more rough fracture surface with evidence of crack-tip pinning and bowing indicates that more energy is absorbed during fracture, and it could also be seen as a confirmation of the higher mechanical properties. It should be noted,

however, that the resolution of the scanning electron micrographs is too low to detect any energy absorbing mechanisms during fracture at the nano-level. In fact, the resolution is too low to detect any individual nanoparticles.

4.4 Mathematical modelling

The experimentally measured tensile modulus of elasticity for both types of alumina nanofillers was compared to mathematical models. The Young's modulus in the direction of the applied load was calculated. The necessary material parameters used as input for the analyses are given in Section 2.1, and the results are displayed in (Figure 10). The experimental data points in the plots are taken from (Table 2) and (Table 3), using the nominal values for the volume fractions.

Several models have been developed for describing the effective properties of short-fibre composites, such as rule of mixtures models and the Halpin-Tsai models [26]. Some of these models can also be applied to nanocomposites, which is the case for the rule of mixtures model by Fidelius *et al.* [27]. For some of the above mentioned models, the fibres are assumed to be aligned, whereas others take into account a random distribution of the fibre-like inclusions [28].

The Mori-Tanaka method [29] is another well known approach, which is applicable for describing composites with inclusions of ellipsoidal shape. Models that apply the Mori-Tanaka method to both aligned and randomly oriented inclusions of different shapes have been developed, and analytical expressions for the elastic modulus of aligned and randomly oriented ellipsoidal particles of certain shapes have been derived [30-33]. A general derivation of the Mori-Tanaka model, including all ellipsoidal shapes, and both aligned and randomly oriented inclusions, has been presented by Fisher and Brinson [34]. In this paper, the model results for the randomly oriented fibre-like inclusions are based on this latter approach alone.

The Mori-Tanaka model for spherical alumina particles is shown in (Figure 10(a)). For the spherical particles the aspect ratio equals one, but curves have also been plotted for particles with a shape that deviates slightly from the spherical, that is, a prolate shape with an aspect ratio of 2, and an oblate shape with an aspect ratio of 0.5. Particle alignment is assumed so that one is able to use the same model as for spherical particles, without the introduction of additional calculations for randomization. The prolate and oblate shapes describe, in some sense, the stiffness for two "extreme" orientations of the particles, compared to a random distribution. The curves may thus be seen as upper and lower boundaries of the Young's modulus in this case. As can be seen, the agreement is very good for the model and the curve for spherical particles employing the bath sonication ("NT-50nm-bath"), despite the observation of significant agglomeration in these composites. On the other hand, the composite where the particles were dispersed using the horn ("NT-50nm-horn"), obtaining better dispersion of the particles, deviates significantly especially for low concentrations of alumina, giving a much higher modulus than what is indicated by the modelling. The Mori-Tanaka models employed here assume that the particles are fully dispersed. These observations suggest that the correlation between the experimental results and the models needs to be further investigated.

The model results for the alumina whiskers (i.e. fibre-like inclusions) are shown in (Figure 10(b)). The aspect ratio of the whiskers is in this case set to 100. In addition, a curve for the randomly oriented fibre needles (aspect ratio $\rightarrow \infty$) has been included. As can been seen from the plot, the models agree well with the experimental results at 0.035 vol%. However, all the models underestimate the stiffness of composites at lower concentrations, and they all, except for the Weng-Sun model, overestimate the stiffness at higher concentrations. This behaviour may be related to the varying degree of

dispersed and agglomerated alumina in the composites, which is a factor that should be taken into account in future modelling.

4.5 Discussion

Both tensile testing and DMA measurements confirmed that the mechanical properties of an epoxy polymer can be improved by adding alumina nanofillers of different shapes. For comparison, in the study by Brown and Ellyin [10;11] both finely dispersed nanoalumina and agglomerated clumps of different sizes were observed after dispersion by sonication. Nevertheless, the material properties were improved upon reinforcement of epoxy with alumina. In another study by Gilbert *et al.* [35], spherical 50 nm particles and whiskers with a diameter of 2-4 nm were added to epoxy based adhesives. These alumina fillers may be very similar, or identical, to the alumina fillers used in the present study. Little detail is given about the dispersion method used, except that the alumina and curing agent were mixed under high shear. This may not be sufficient to give well dispersed individual particles and whiskers, but the authors still found that the addition of alumina could improve the peel and shear strength of the adhesive. In the present study, the tensile modulus of the specimen "NT-whiskers-bath" containing as little as 0.1 wt% whiskers, which corresponds to 0.035 vol%, increased the tensile modulus from 3120 MPa to 3310 MPa. There could be several explanations for this observation. SEM indicated that the composite contained a relatively low concentration of agglomerates, owing to the low concentration of alumina. Even if these agglomerates are acting as rigid particles, the high increase is not expected. In comparison, a simple rule of mixtures analysis [26] anticipates a tensile modulus of 3250 MPa. Neither did the numerical modelling in Section 4.4 anticipate this high increase.

On the other hand, a higher degree of dispersion of the alumina, resulting in the formation of more dispersed individual whiskers, could result in a positive effect.

Several of the techniques used in this study, including optical microscopy and DCS particle size characterisations of dispersions, as well as SEM of fracture surfaces, indicated that horn sonication results in a higher degree of dispersion, or at least smaller agglomerates, compared to bath sonication. Unexpectedly then, the sonication using the horn gave a lower value for the tensile modulus at 0.1 wt% whiskers ("NT-whiskers-horn"). The energy input using the horn is higher, and a higher degree of dispersion is then expected. One possible negative effect of the higher energy input that this result may highlight, is that a shortening of the whiskers due to breaking may occur during the high-shear sonication process. This lowers the aspect ratio of the whiskers, making them less efficient in stiffening the epoxy polymer. There is no experimental evidence for any of these explanations, and so, without further investigation there is an uncertainty associated with them.

Some sedimentation of large agglomerates was observed during the preparation of the nanocomposite test specimens, as described in Section 3.1. These sediments were not included in the test specimens, and the alumina content in the specimens may therefore deviate somewhat from the nominal content of alumina. Attempts were made to determine the alumina content using thermogravimetric analyses, but the concentration is so low that accurate measurements could not be performed. However, elemental analyses of the test specimens have indicated that up to one third of the alumina may have sedimented in some cases. The actual fraction of alumina may therefore be lower than the nominal values presented in (Table 2) and (Table 3).

The presence of agglomerates in the nanocomposites shows that the power input during the sonication of the alumina/anhydride dispersions in this study was not sufficient to completely break up the agglomerates shown in (Figure 2). However, although agglomerates were observed after both dispersion methods, the horn sonicator

was much more efficient in breaking up the agglomerates. The relative amounts of dispersed and agglomerated whiskers in the composites have not been quantified, but the result was nevertheless an increase in stiffness even when agglomerates were present.

A high degree of dispersion of the nanoparticles is usually considered important to obtain improved material properties of the nanocomposites. In the case that a high degree of dispersion is obtained during the sonication, the effect of this may be partly reversed by re-agglomeration. Re-agglomeration of individual dispersed nanoparticles, in this case alumina, may take place, particularly since no surfactant was used to stabilise the individual alumina particles in the anhydride dispersions. It has been shown that the use of surfactants, at least in some solvents, is necessary to obtain stable dispersions [36]. Re-agglomeration of the spherical 50 nm alumina particles was also indicated by the differential sedimentation analysis of one alumina/anhydride dispersion, see Section 3.2.

In the tensile testing in this study, positive effects on the strength and the elongation at break of the nanocomposites reinforced with the surface-modified spherical 50 nm alumina particles were observed. There are at least two possible explanations for the better performance of the surface-modified particles. First, organofunctional silanes are widely used as coupling agents to enhance the interfacial properties of composite materials and adhesive joints. The improved interfacial strength, and thus the improved particle/matrix adhesion, could enhance the macroscopic mechanical properties, such as the tensile strength [1]. The mechanisms of improvement of the interfacial properties between aluminium oxides (e.g. alumina) and epoxy polymers when using the GPS silane are regarded as quite well understood [37]. The GPS silane has a hydrolysable group ($–OCH_3$) and an organofunctional group (an

epoxy). The hydrolysable group can enable the formation of strong Al–O–Si bonds to the alumina surface, and the epoxy group can react with the anhydride hardener used for curing of the epoxy resin. Hence, the density of strong, covalently linked bonds between the oxide and the epoxy polymer is increased. Second, prior to the surface treatment, the particulate filler was pre-dispersed in toluene using the bath sonicator. Although the solvent was subsequently removed and the filler dried, this may have resulted in more loosely bound agglomerates. The pre-dispersion may then have led to a higher degree of dispersion in the epoxy polymer. The different state of the non-modified and surface-modified fillers in the alumina/anhydride dispersions directly after mixing and after sonication can be observed in (Figure 4). The agglomerates in the surface-modified filler are not present after sonication, and as a whole, fewer agglomerates are observed compared to the non-modified particulate filler.

5 Conclusions

Nanosized alumina fillers in the shape of fibre-like whiskers and spherical 50 nm particles were added to an epoxy polymer. The alumina fillers were initially in a high agglomerated state, and two different sonication methods were used for dispersion in the anhydride hardener of the epoxy polymer. The agglomerates of the spherical 50 nm particles were less rigid, and it was shown from particle size analysis that they could be dispersed to form individual particles. Horn sonication gave the highest specific energy input to the alumina/anhydride dispersions, resulting in a higher degree of dispersion. Therefore, fewer agglomerates were observed in some of the nanocomposites prepared by horn sonication, compared to those prepared by bath sonication.

Mechanical testing revealed that the stiffness, or the modulus, of the epoxy polymer was improved when alumina was added, even at very low concentrations of alumina. This effect was observed also when agglomerates of the alumina were present

in the nanocomposites. Generally, the whiskers seemed to improve the modulus more than the 50 nm particles, although a high stiffness could be obtained when dispersing the particles using the horn. For low concentrations of alumina, the experimental results in some cases agreed quite well with mathematical models.

The strength and the elongation at break of the nanocomposites were typically reduced or maintained at the same level as the neat epoxy polymer. However, the addition of surface-modified alumina particles had a positive effect compared to adding non-treated particles. Possible reasons for this are improved interfacial strength and/or better dispersion of the particles after the surface treatment.

Thermal analysis showed that there was not a significant difference in the glass transition temperature between the neat epoxy polymer and the nanocomposites.

Acknowledgements

The authors would like to acknowledge F.K. Hansen (University of Oslo), J.R. Nilssen, I.V. Johnsen (FFI), W.R. Glomm and S.M.N. Stavnes (Norwegian University of Science and Technology) for their assistance in the preparation of this manuscript.

References

[1] Fu SY, Feng XQ, Lauke B, Mai YW. Effects of particle size, particle/matrix interface adhesion and particle loading on mechanical properties of particulate-polymer composites. Compos. Part B-Eng. 2008;39:933-961.

[2] Ma PC, Siddiqui NA, Marom G, Kim JK. Dispersion and functionalization of carbon nanotubes for polymer-based nanocomposites: A review. Compos. Part A-Appl. S. 2010;41:1345-1367.

[3] Moniruzzaman M, Winey KI. Polymer nanocomposites containing carbon nanotubes. Macromolecules 2006;39:5194-5205.

[4] Thostenson ET, Li CY, Chou TW. Nanocomposites in context. Compos. Sci. Technol. 2005;65:491-516.

[5] Paul DR, Robeson LM. Polymer nanotechnology: Nanocomposites. Polymer 2008;49(15):3187-3204.

[6] Johnsen BB, Kinloch AJ, Mohammed RD, Taylor AC, Sprenger S. Toughening mechanisms of nanoparticle-modified epoxy polymers. Polymer 2007;48:530-541.

[7] Zou H, Wu SS, Shen J. Polymer/silica nanocomposites: Preparation, characterization, properties, and applications. Chem. Rev. 2008;108:3893-3957.

[8] Zhang H, Zhang Z, Friedrich K, Eger C. Property improvements of in situ epoxy nanocomposites with reduced interparticle distance at high nanosilica content. Acta Mater. 2006;54:1833-1842.

[9] Nairn JA. Aspect ratio requirements for nanotube-reinforced, polymer matrix composites. Compos. Part A-Appl. S. 2011;42:1850-1855.

[10] Brown GM, Ellyin F. Assessing the predictive capability of two-phase models for the mechanical behavior of alumina/epoxy nanocomposites. J. Appl. Polym. Sci. 2005;98:869-879.

[11] Brown GM, Ellyin F. Mechanical properties and multiscale characterization of nanofiber-alumina/epoxy nanocomposites. J. Appl. Polym. Sci. 2011;119:1459-1468.

[12] Miyagawa H, Mohanty A, Drzal LT, Misra M. Effect of clay and alumina-nanowhisker reinforcements on the mechanical properties of nanocomposites from biobased epoxy: A comparative study. Ind. Eng. Chem. Res. 2004;43:7001-7009.

[13] Zhao S, Schadler LS, Duncan R, Hillborg H, Auletta T. Mechanisms leading to improved mechanical performance in nanoscale alumina filled epoxy. Compos. Sci. Technol. 2008;68:2965-2975.

[14] Yang F, Bogdanova I, Wang KG, Nelson GL. Reinforcement in aromatic polymer nanocomposites. Paper presented at: SAMPE '07; 2007 June 3-5; Baltimore, Maryland, USA.

[15] Wetzel B, Rosso P, Haupert F, Friedrich K. Epoxy nanocomposites - fracture and toughening mechanisms. Eng. Fract. Mech. 2006;73:2375-2398.

[16] Richardson DW. Modern ceramic engineering: Properties, processing, and use in design. New York, USA: Marcel Dekker, Inc.; 1982.

[17] Engineered materials handbook: Ceramics and Glasses. Materials Park, Ohio, USA: ASM International; 1991.

[18] Frømyr TR, Hansen FK, Olsen T. The optimum distribution of carbon nanotubes for epoxy nanocomposites: Evolution of the particle size distribution by ultrasonic treatment. J. Nanotechnol. 2012. Available from: http://www.hindawi.com/journals/jnt/2012/545930/

[19] Tsubokawa N, Maruyama K, Sone Y, Shimomura M. Graft-polymerization of acrylamide from ultrafine silica particles by use of a redox system consisting of ceric ion and reducing groups on the surface. Polym. J. 1989;21:475-481.

[20] Abboud M, Turner M, Duguet E, Fontanille M. PMMA-based composite materials with reactive ceramic fillers .1. Chemical modification and characterisation of ceramic particles. J. Mater. Chem. 1997;7:1527-1532.

[21] Gupta S, Ramamurthy PC, Madras G. Covalent grafting of polydimethylsiloxane over surface-modified alumina nanoparticles. Ind. Eng. Chem. Res. 2011;50:6585-6593.

[22] ASTM D792-08 Standard Test Methods for Density and Specific Gravity (Relative Density) of Plastics by Displacement.

[23] Kass MD. Ultrasonically induced fragmentation and strain in alumina particles. Mater. Lett. 2000;42:246-250.

[24] Betts JN, Johnson MG, Rygiewicz PT, King GA, Andersen CP. Potential for metal contamination by direct sonication of nanoparticle suspensions. Environ. Toxicol. Chem. 2013;32.

[25] Cantwell WJ, Roulin-Moloney AC. Fractography and failure mechanisms of unfilled and particulate filled epoxy resins. In: Roulin-Moloney AC, editor. Fractography and failure mechanisms of polymers and composites. London, United Kingdom: Elsevier Applied Science; 1989. p. 233-290.

[26] Agarwal BD, Broutman LJ, Chandrashekhara K. Analysis and performance of fiber composites. Hoboken, New Jersey, USA: John Wiley & Sons; 2006.

[27] Fidelus JD, Wiesel E, Gojny FH, Schulte K, Wagner HD. Thermomechanical properties of randomly oriented carbon/epoxy nanocomposites. Compos. Part A-Appl. S. 2005;36:1555-1561.

[28] Thorvaldsen T, Johnsen BB, Osnes H. Modelling of nanofibre composites. Paper presented at: 14th European Conference on Composite Materials; 2010 June 7-10; Budapest, Hungary.

[29] Mori T, Tanaka K. Average stress in matrix and average elastic energy of materials with misfitting inclusions. Acta Metall. 1973;21:571-574.

[30] Tandon GP, Weng GJ. The effect of aspect ratio of inclusions on the elastic properties of unidirectionally alligned composites. Polym. Compos. 1984;5:327-333.

[31] Qiu YP, Weng GJ. On the application of Mori-Tanaka's theory involving transversely isotropic spheroidal inclusions. Int. J. Eng. Sci. 1990;28:1121-1137.

[32] Weng GJ. Some elastic properties of reinforced solids, with special reference to isotropic ones containing spherical inclusions. Int. J. Eng. Sci. 1984;22:845-856.

[33] Tandon GP, Weng GJ. Average stress in the matrix and effective moduli of randomly oriented composites. Compos. Sci. Technol. 1986;27:111-132.

[34] Fisher F, Brinson LC. Nanomechanics of nanoreinforced polymers. In: Rieth M, Schommers W, editors. Handbook of theoretical and computational nanotechnology: Functional nanomaterials, nanoparticles, and polymer design. American Scientific Publishers; 2006. p. 253-360.

[35] Gilbert EN, Hayes BS, Seferis JC. Nano-alumina modified epoxy based film adhesives. Polym. Eng. Sci. 2003;43:1096-1104.

[36] Liu JC, Jean JH, Li CC. Dispersion of nano-sized alumina powder in non-polar solvents. J. Am. Ceram. Soc. 2006;89:882-887.

[37] Johnsen BB, Olafsen K, Stori A. Reflection-absorption FT-IR studies of the specific interaction of amines and an epoxy adhesive with GPS treated aluminium surfaces. Int. J. Adhes. Adhes. 2003;23:157-165.

TABLES

Table 1. A list of the different types of nanocomposites.

Specimen denotation	Type of nano-filler	Method of sonication	Surface treatment
Epoxy	n/a	n/a	n/a
NT-whiskers-bath	Whiskers	Bath	No
NT-whiskers-horn	Whiskers	Horn	No
NT-50nm-bath	Spherical particles	Bath	No
NT-50nm-horn	Spherical particles	Horn	No
GPS-50nm-bath	Spherical particles	Bath	Yes
GPS-50nm-horn	Spherical particles	Horn	Yes

Table 2. Results from the tensile testing of the nanocomposites where the alumina fillers were dispersed using the bath sonicator.

Type of reinforcement	Content of alumina		Tensile modulus, E	Tensile strength, σ_{max}	Tensile strain, ε_{max}
	(wt%)	(vol%)	(MPa)	(MPa)	(%)
Epoxy	n/a	n/a	3120 ± 110	89 ± 11	7.4 ± 0.9
NT-whiskers	0.1	0.035	3310 ± 140	90 ± 1	5.8 ± 0.2
	1.0	0.350	3360 ± 110	89 ± 1	5.1 ± 0.2
	3.0	1.060	3450 ± 170	80 ± 7	3.6 ± 0.8
	5.0	1.730	3540 ± 130	81 ± 3	3.4 ± 0.3
NT-50nm	1.0	0.350	3150 ± 100	79 ± 3	3.5 ± 0.3
	4.0	1.385	3220 ± 130	76 ± 2	3.1 ± 0.2
GPS-50nm	3.0	1.060	3290 ± 130	88 ± 11	5.8 ± 0.8

Table 3. Results from the tensile testing of the nanocomposites where the alumina fillers were dispersed using the horn sonicator.

Type of reinforcement	Content of alumina		Tensile modulus, E	Tensile strength, σ_{max}	Tensile strain, ε_{max}
	(wt%)	(vol%)	(MPa)	(MPa)	(%)
Epoxy	n/a	n/a	3120 ± 110	89 ± 11	7.4 ± 0.9
NT-whiskers	0.1	0.035	3210 ± 190	90 ± 3	4.9 ± 1.1
	1.0	0.345	3390 ± 120	79 ± 3	3.3 ± 0.3
	2.9	1.025	3360 ± 140	84 ± 6	3.6 ± 0.6
NT-50nm	1.0	0.345	3400 ± 190	88 ± 8	4.5 ± 1.1
	2.9	1.025	3240 ± 70	85 ± 6	4.0 ± 1.0
GPS-50nm	1.0	0.345	3130 ± 60	93 ± 1	5.6 ± 0.7

FIGURE CAPTIONS

Figure 1. The cylindrical shaped test specimen used for tensile testing of the neat epoxy polymer and the nanocomposites.

Figure 2. Scanning electron micrographs of the as-received agglomerated alumina nanofillers: (a-b) Fibre-like whiskers, (c-d) spherical 50 nm particles, and (e) surface-modified spherical 50 nm particles.

Figure 3. Example of alumina/anhydride dispersions used to prepare the nanocomposites. (a) Dispersion containing 6.0 wt% spherical 50 nm particles 30 min after mixing, and (d) the same dispersion 30 min after bath sonication.

Figure 4. Microscopy of the alumina/anhydride dispersions similar to those used to prepare the nanocomposites after mixing, after bath sonication, and after horn sonication, respectively: (a-c) 6.0 wt% whiskers, (d-f) 6.0 wt% spherical particles, and (g-i) 3.0 wt% surface-modified spherical particles. The width of each image is 1.25 mm.

Figure 5. Particle size distributions of spherical alumina particles with different dispersion procedures. The specific sonication energy input is given in brackets. A 0.1 wt% suspension in MIBK is depicted after (1) 10 min bath sonication [0.08 kJ/g], (2) 1 hour bath sonication [0.5 kJ/g], and (3) 1 hour bath sonication plus an additional 10 min horn sonication at 20% amplitude [3.7 kJ/g]. (4) A 2.0 wt% alumina/anhydride dispersion after 1 hour horn sonication at 20% amplitude [3.7 kJ/g].

Figure 6. Mechanical properties of the nanocomposites: (a) Tensile modulus, E, and (b) tensile strength, σ_{max}.

Figure 7. Scanning electron micrographs of the neat epoxy fracture surface after tensile testing.

Figure 8. Scanning electron micrographs of nanocomposite fracture surfaces after tensile testing.

Figure 9. Dynamic mechanical analysis of selected nanocomposites: (a) Storage modulus, E', and (b) loss modulus, E''.

Figure 10. Modelling of the nanocomposites: (a) Results for the spherical 50 nm particles, and (b) results for the fibre-like whiskers.

DOI til publisert versjon/DOI to published version: 10.1080/15685543.2013.815603

FIGURES

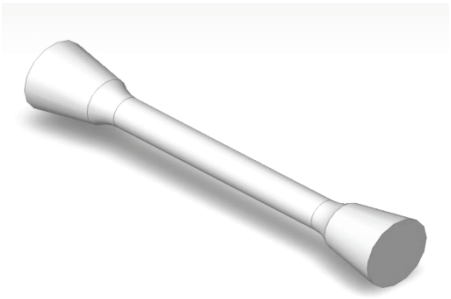

Figure 1. The cylindrical shaped test specimen used for tensile testing of the neat epoxy polymer and the nanocomposites.

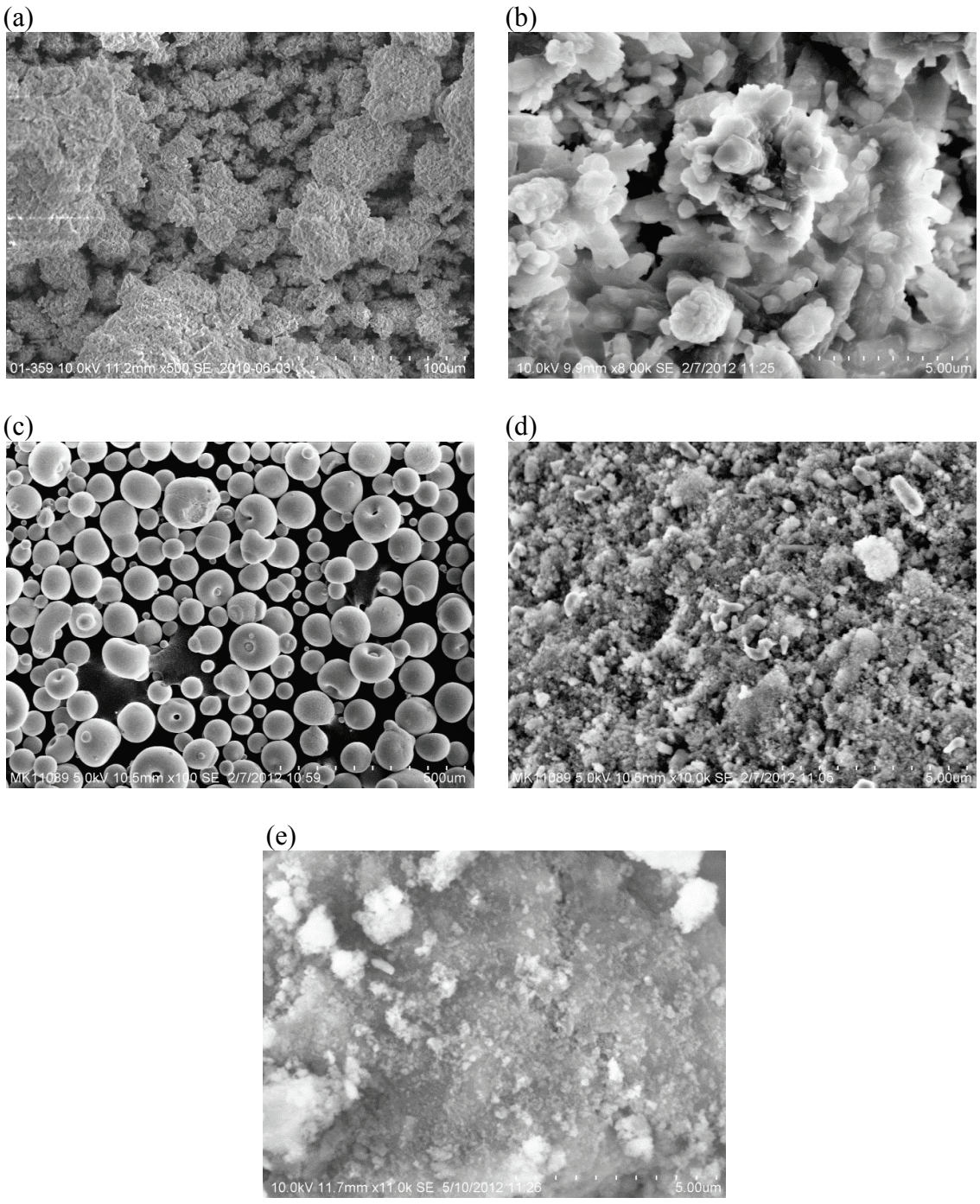

Figure 2. Scanning electron micrographs of the as-received agglomerated alumina nanofillers: (a-b) Fibre-like whiskers, (c-d) spherical 50 nm particles, and (e) surface-modified spherical 50 nm particles.

(a) (b)

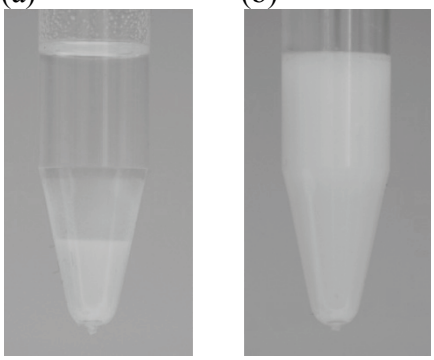

Figure 3. Example of alumina/anhydride dispersions used to prepare the nanocomposites. (a) Dispersion containing 6.0 wt% spherical 50 nm particles 30 min after mixing, and (d) the same dispersion 30 min after bath sonication.

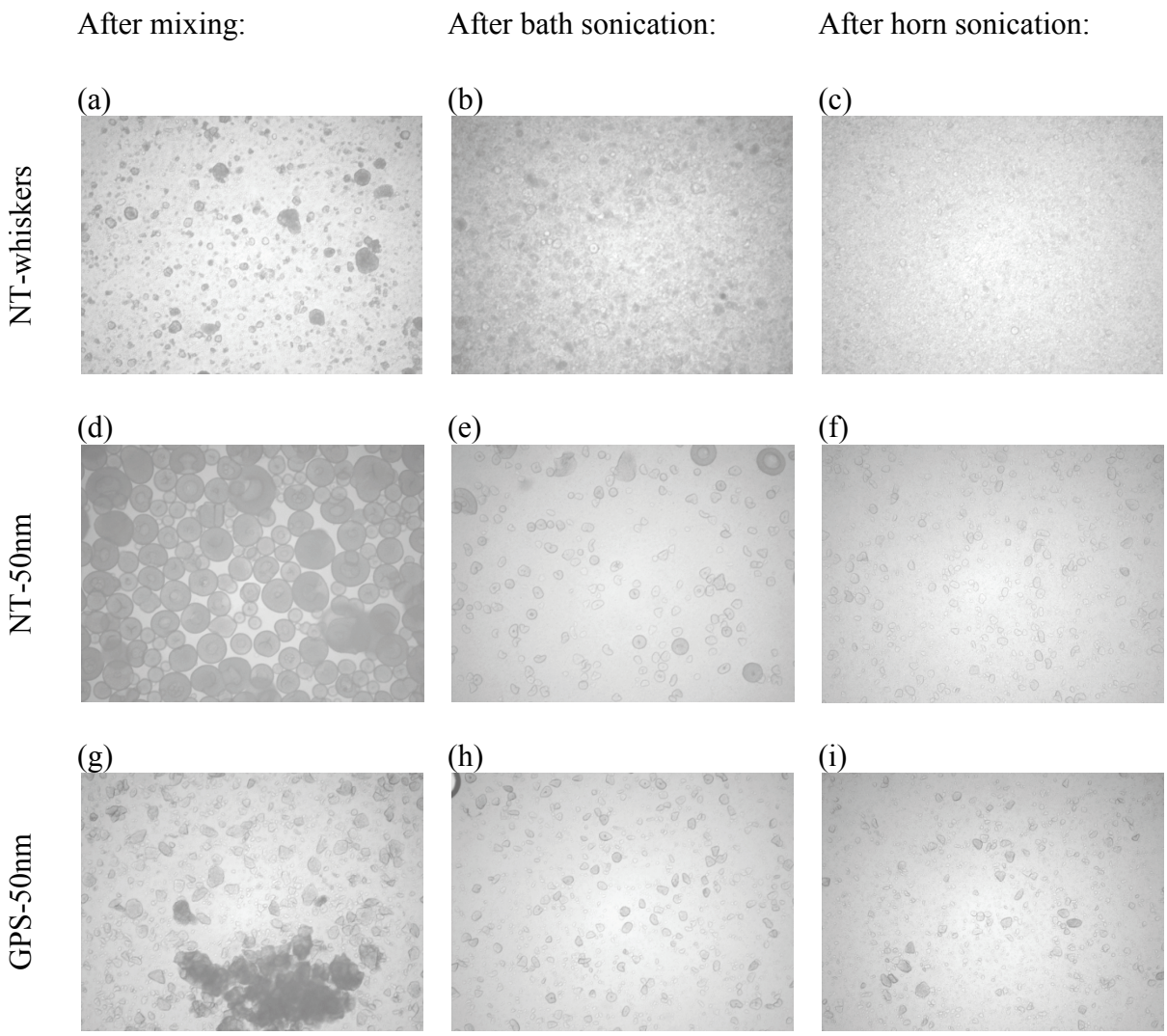

Figure 4. Microscopy of the alumina/anhydride dispersions similar to those used to prepare the nanocomposites after mixing, after bath sonication, and after horn sonication, respectively: (a-c) 6.0 wt% whiskers, (d-f) 6.0 wt% spherical particles, and (g-i) 3.0 wt% surface-modified spherical particles. The width of each image is 1.25 mm.

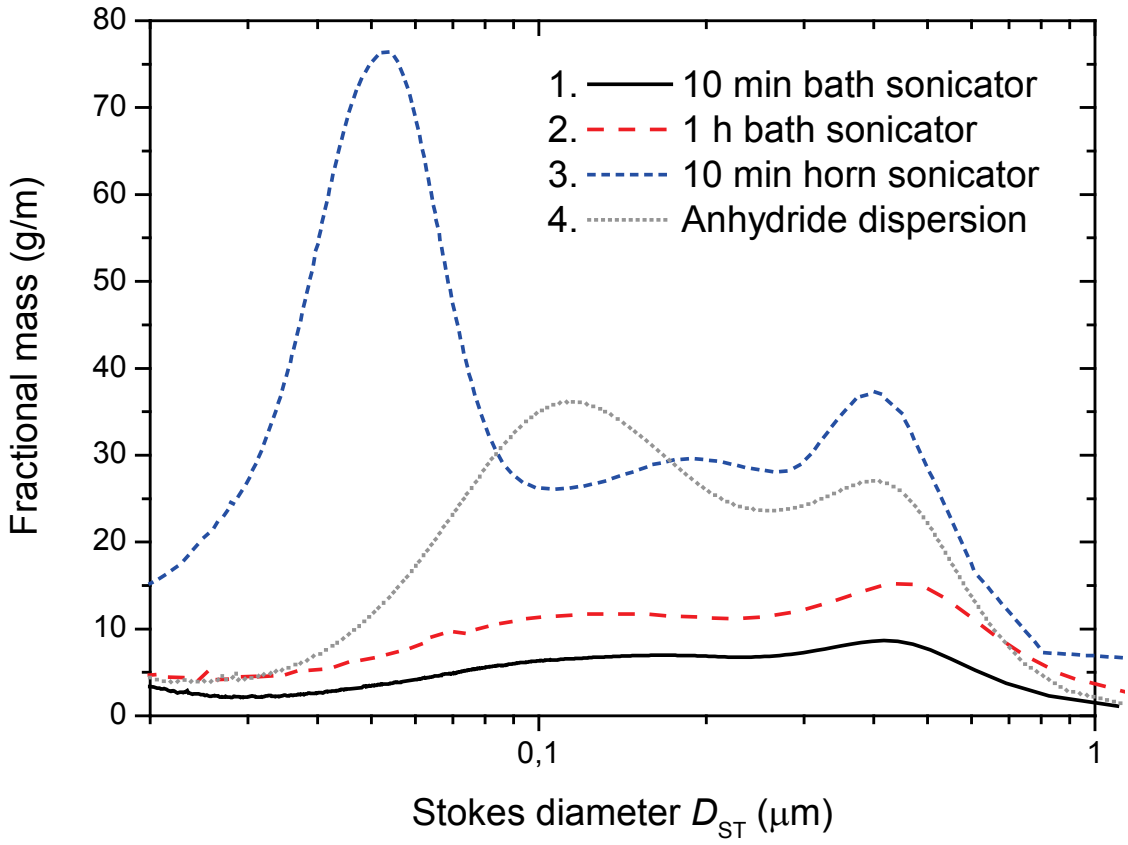

Figure 5. Particle size distributions of spherical alumina particles with different dispersion procedures. The specific sonication energy input is given in brackets. A 0.1 wt% suspension in MIBK is depicted after (1) 10 min bath sonication [0.08 kJ/g], (2) 1 hour bath sonication [0.5 kJ/g], and (3) 1 hour bath sonication plus an additional 10 min horn sonication at 20% amplitude [3.7 kJ/g]. (4) A 2.00 wt% alumina/anhydride dispersion after 1 hour horn sonication at 20% amplitude [3.7 kJ/g].

DOI til publisert versjon/DOI to published version: 10.1080/15685543.2013.815603

(a)

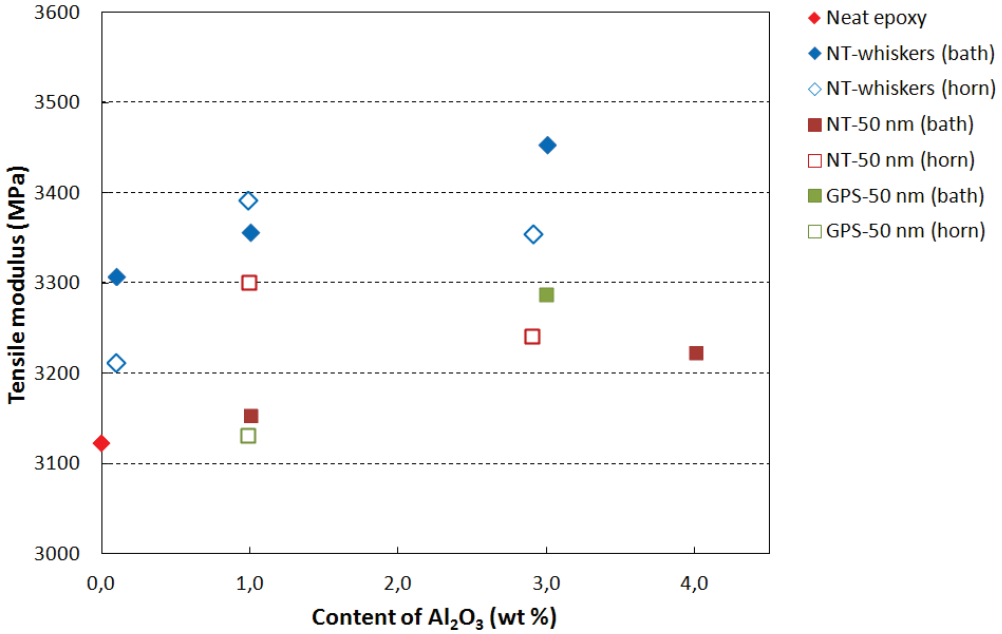

(b)

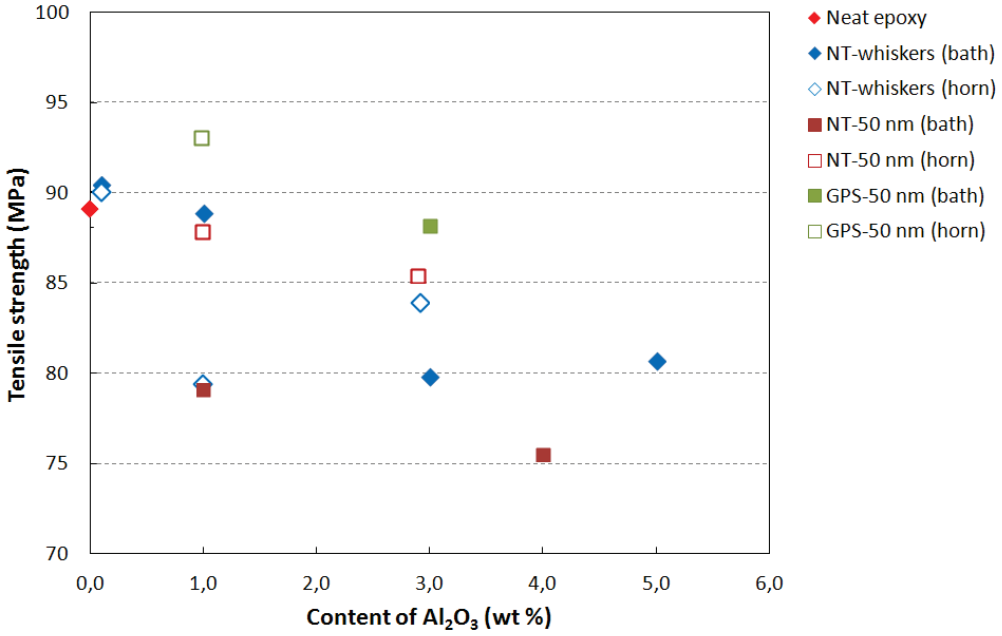

Figure 6. Mechanical properties of the nanocomposites: (a) Tensile modulus, E, and (b) tensile strength, σ_{max}.

DOI til publisert versjon/DOI to published version: 10.1080/15685543.2013.815603

(a) (b)

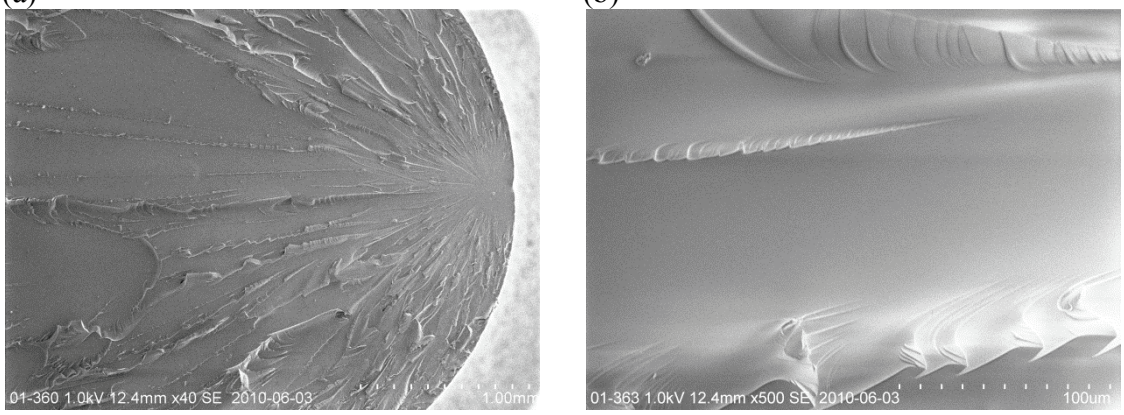

Figure 7. Scanning electron micrographs of the neat epoxy fracture surface after tensile testing.

DOI til publisert versjon/DOI to published version: 10.1080/15685543.2013.815603

(a) NT-50nm-bath (1.0 wt%)

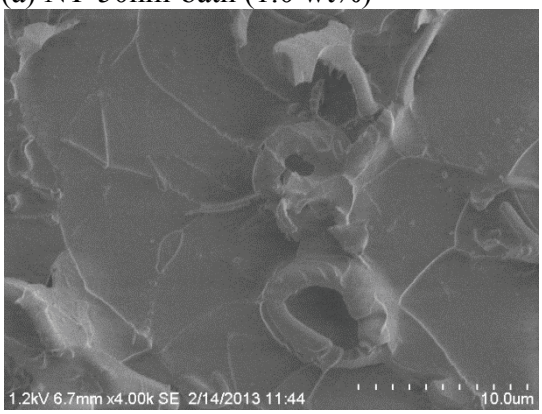

(b) NT-50nm-horn (1.0 wt%)

(c) NT-whiskers-bath (3.0 wt%)

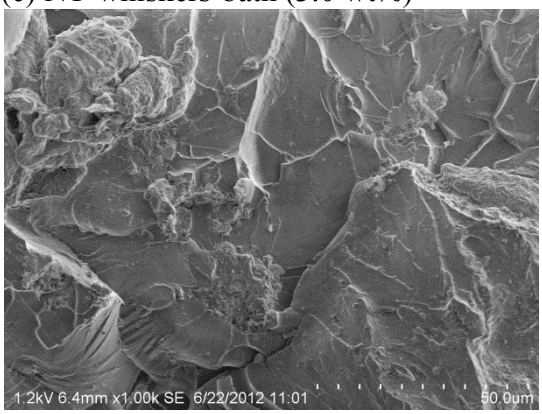

(d) NT-whiskers-horn (2.9 wt%)

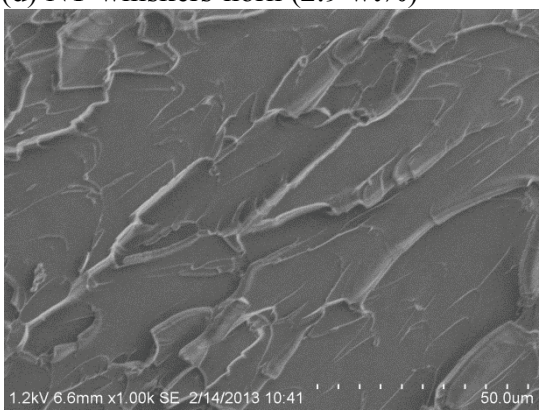

(e) GPS-50nm-bath (3.0 wt%)

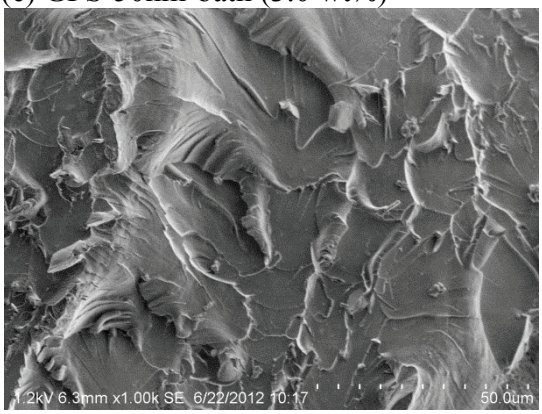

(f) GPS-50nm-horn (1.0 wt%)

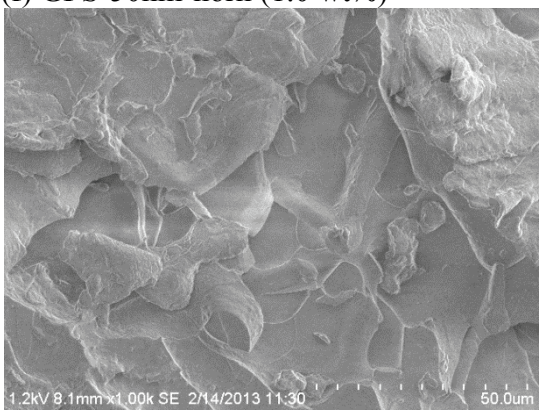

Figure 8. Scanning electron micrographs of nanocomposite fracture surfaces after tensile testing.

DOI til publisert versjon/DOI to published version: 10.1080/15685543.2013.815603

(a)

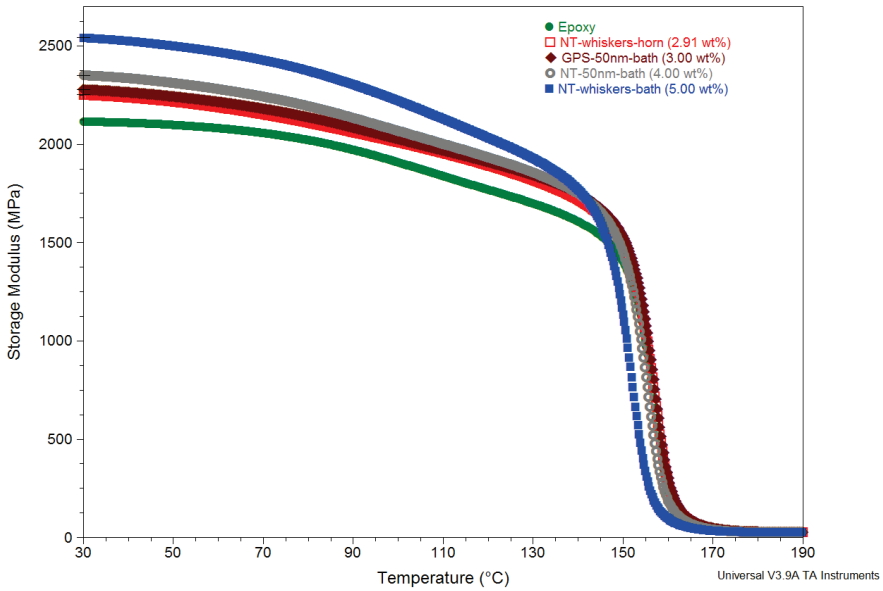

(b)

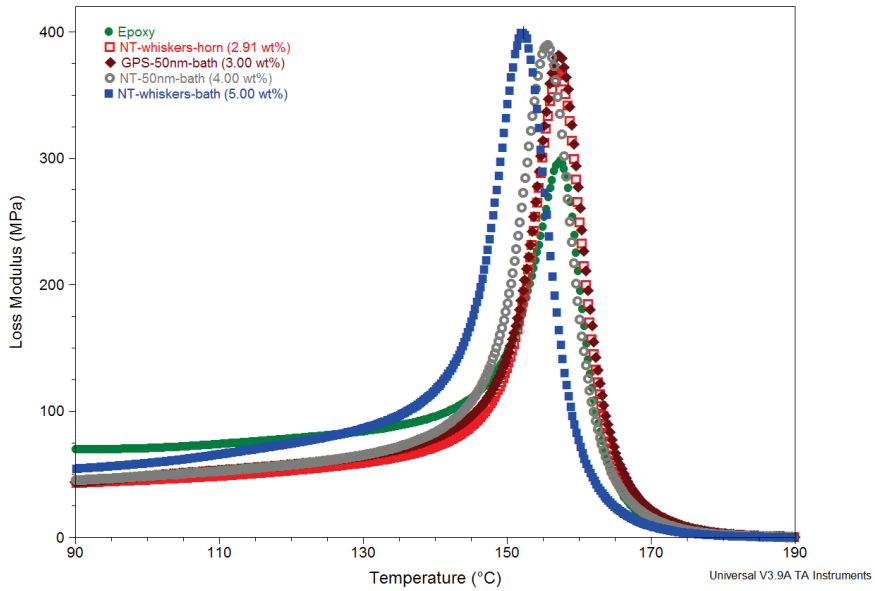

Figure 9. Dynamic mechanical analysis of selected nanocomposites: (a) Storage modulus, E', and (b) loss modulus, E''.

Dette er en postprint-versjon/This is a postprint version.
DOI til publisert versjon/DOI to published version: 10.1080/15685543.2013.815603

(a)

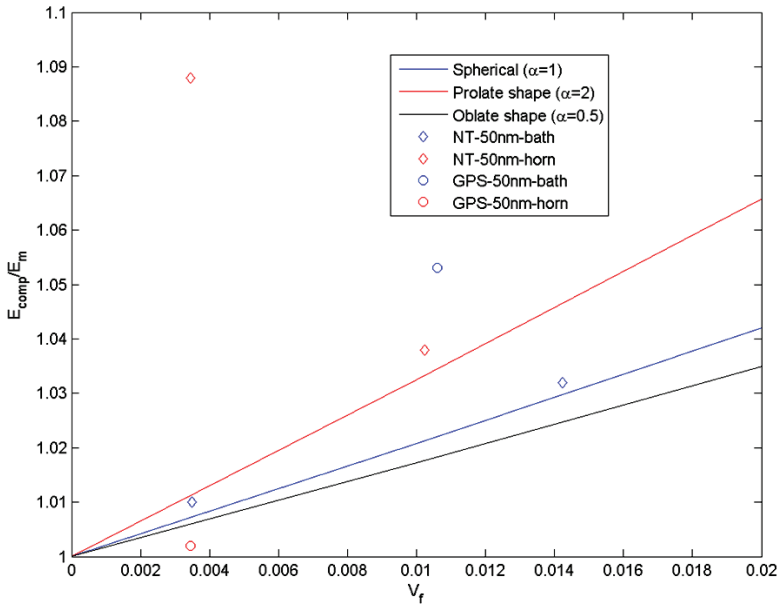

(b)

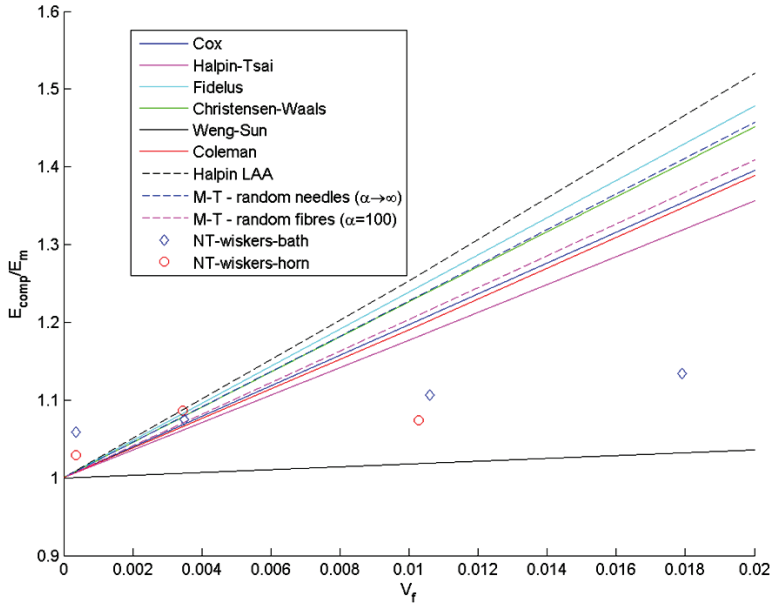

Figure 10. Modelling of the nanocomposites: (a) Results for the spherical 50 nm particles, and (b) results for the fibre-like whiskers.

Dette er en postprint-versjon/This is a postprint version.
DOI til publisert versjon/DOI to published version: 10.1080/15685543.2013.815603